Smart Structures and Systems, *Vol. 16, No. 4 (2015) 623-640*
DOI: http://dx.doi.org/10.12989/sss.2015.16.4.623

Modelling and experimental investigations on stepped beam with cavity for energy harvesting

A. Rami Reddy[a], M. Umapathy[*], D. Ezhilarasi[b] and G. Uma[c]

Department of Instrumentation and Control Engineering, National Institute of Technology, Tiruchirappalli-620015, TamilNadu, India

(Received September 10, 2014, Revised February 3, 2015, Accepted February 5, 2015)

Abstract. This paper presents techniques to harvest higher voltage from piezoelectric cantilever energy harvester by structural alteration. Three different energy harvesting structures are considered namely, stepped cantilever beam, stepped cantilever beam with rectangular and trapezoidal cavity. The analytical model of three energy harvesting structures are developed using Euler-Bernoulli beam theory. The thickness, position of the rectangular cavity and the taper angle of the trapezoidal cavity is found to shift the neutral axis away from the surface of the piezoelectric element which in turn increases the generated voltage. The performance of the energy harvesters is evaluated experimentally and is compared with regular piezoelectric cantilever energy harvester. The analytical and experimental investigations reveal that, the proposed energy harvesting structures generate higher output voltage as compared to the regular piezoelectric cantilever energy harvesting structure. This work suggests that through simple structural modifications higher energy can be harvested from the widely reported piezoelectric cantilever energy harvester.

Keywords: energy harvesting; piezoelectric; stepped beam; rectangular cavity; trapezoidal cavity

1. Introduction

Harvesting energy from the mechanical vibrations in the environment using piezoelectric transducer based approach has been the focus of many recent investigations. The applications of energy harvester include wireless sensor, portable electronic devices, implanted biomedical devices, battery charging or replacement operation, microelectromechanical systems, health monitoring, MAV applications, cameras etc (Levron *et al*. 2011, Ferrari *et al*. 2009, Barker *et al*. 2011, Magoteaux *et al.* 2008, Abdelkefi *et al.* 2013). Most of the energy harvesters reported in literature consists of a cantilever beam structure with one or more piezoelectric transducers (Sodano and Inman 2004, Priya 2007). In very recent years, efforts are made by researchers to improve the harvested power from the piezoelectric energy harvester by the way of structural tailoring, structural modification, attaching additional mass and so on.

Carlos *et al*. (2009) derived an electromechanically coupled finite element (FE) plate model for

*Corresponding author, Professor, E-mail: umapathy@nitt.edu
[a] Research Scholar, E-mail: rreddyar@gmail.com
[b] Assistant Professor, E-mail: ezhil@nitt.edu
[c] Associate Professor, E-mail: guma@nitt.edu

http://www.techno-press.org/?journal=sss&subpage=8 ISSN: 1738-1584 (Print), 1738-1991 (Online)

piezoelectric energy harvesting system using base excitations for predicting the electrical power output. The performance of a circular piezoelectric diaphragm energy harvester at resonance frequency is demonstrated by Chen *et al*. (2012). It is shown that the energy from the harvester increases as its resonance frequency decreases. Kim *et al.* (2013) proposed three kinds of hollow plate ceramic harvesters such as square-plate ceramic- type, hexagon-plate ceramic-type and circle-plate ceramic type harvesters and concluded that hexagon-type harvester generates higher voltages using experimental and simulation studies. Li *et al.* (2010) proposed a cantilever piezoelectric power harvester with a curved L-shape proof mass that lowers the fundamental frequency and improves the power density in comparison with conventional cantilever piezoelectric power harvesters. A cantilever piezoelectric energy harvester with an H-shape proof mass comprising of two detached metal blocks with an optimized mass ratio to generate a bending moment at tip which improves the strain distribution along the beam is reported by Guan *et al.* (2013). Abdelkefi *et al.* (2012) have investigated a beam with tip mass structure to harvest energy from multi frequency components with a base excitation and shown the way to extract more energy from three frequency components by adjusting the asymmetry of the tip masses.

Mehraeen *et al.* (2010) have proved that tapered cantilever beams are more effective in generating uniform strain profile over rectangular and trapezoidal beams and resulting in increased harvested power. The harvested energy from the piezoelectric energy harvester is maximized by varying the thickness of the beam along its length which produces more uniform strain distribution along piezoelectric element length (Paquin and St-Amant 2010). Benasciutti *et al.* (2010) proposed vibration energy harvesting system using piezoelectric resonant bimorph beams to convert the environmental vibration into electrical energy. They proposed two trapezoidal configurations, having respectively the wider side clamped or free and shown that considerable gains in power levels are achieved as compared to the rectangular shape beam with equal width. The effects of shape variations of a cantilever beam on its performance as an energy harvester has been investigated by Ben Ayed *et al.* (2013) and concluded that the fundamental natural frequency and mode shape are strongly affected when varying the shape of the multilayered cantilever beam. These energy harvesters with piezoelectric element can generate energy at low-frequency excitations with enhanced power density. The influence of variation in the cross-section, in the natural frequency, mode shapes and amplitude of vibration has been discussed (Ece *et al.* 2007). In this work piezoelectric energy harvesting systems using stepped cantilever beam with rectangular and trapezoidal cavity are designed and developed to improve the harvester performance.

This paper is organized as follows. Section 2 presents description of energy harvesting structures. Modelling of the stepped cantilever beam with rectangular, trapezoidal cavity is presented in Section 3. Section 4 presents the experimental evaluation, results and discussions are presented in Section 5. Conclusions are drawn in Section 6.

2. Description of energy harvesting structures

An energy harvesting structure using stepped cantilever beam with piezoelectric element is considered in this paper. The stepped beam develops higher bending moment than the normal beam and generates higher voltage from the piezoelectric element. Fig. 1(a) shows the stepped beam piezoelectric harvester without cavity. To improve the harvested power, a rectangular cavity is introduced in the stepped beam exactly below the piezoelectric element location as shown in Fig. 1(b). The thickness and position of the rectangular cavity in the stepped beam influences the

neutral axis and the generated voltage. Further to increase the efficiency of energy conversion in the harvester, a trapezoidal cavity is proposed instead of rectangular cavity. The taper angle of the trapezoidal cavity in the stepped beam develops more uniform strain distribution than the beam without cavity and with rectangular cavity and generates higher voltage from the piezoelectric element. To analyze the effect of shape, dimension and position of cavity on the harvested power, six structures having same outer dimension and piezoelectric dimension are considered which are shown in Figs. 1(a)-1(f).

The structures are designed using Aluminium stepped cantilever beam of length L with piezoelectric element of length l which is placed on the top surface of the beam at a distance L_1 from the fixed end. A rectangular cavity of length l is introduced in the stepped beam with different cavity thickness and position from the top surface of the beam to form the structures as shown in Figs. 1(b)-1(d). Similarly a trapezoidal cavity of length l is introduced in the stepped beam as shown in Figs. 1(e)-1(f) with different the taper angle (α).

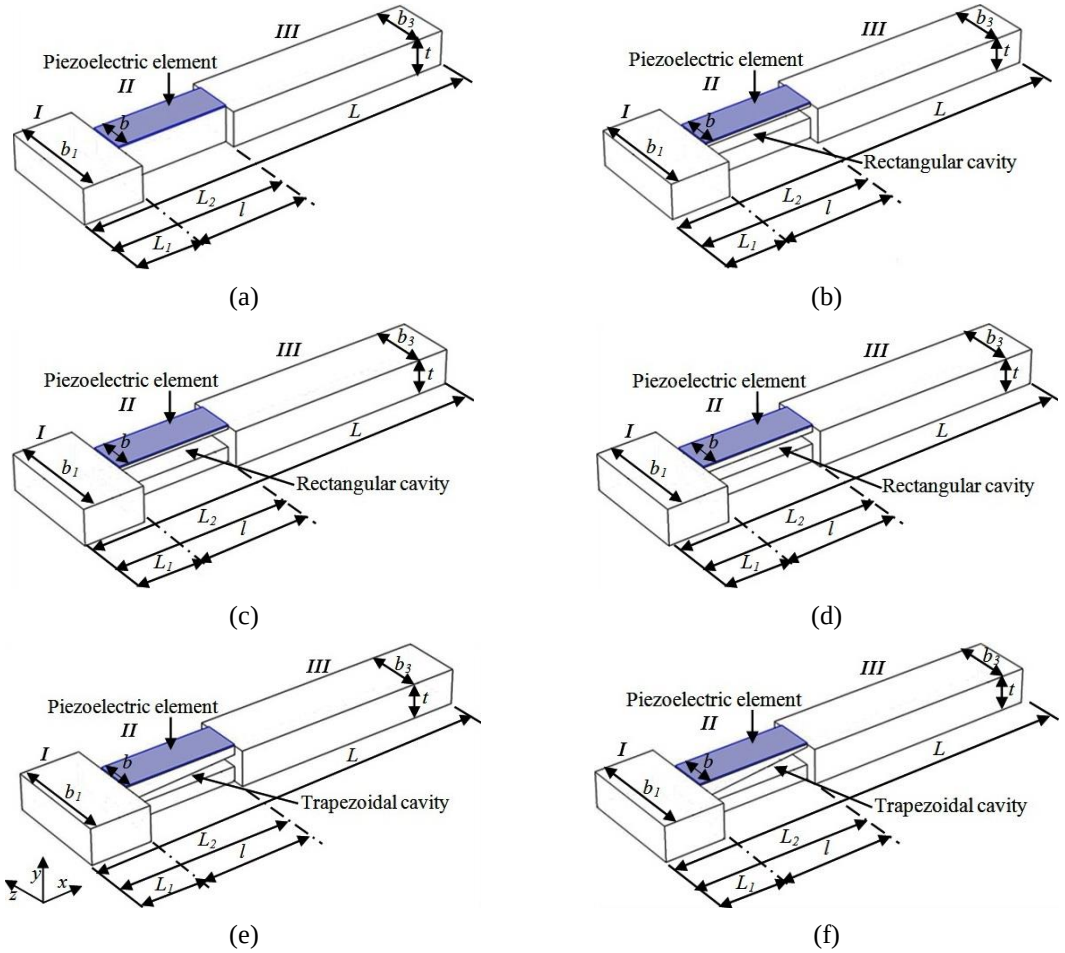

Fig. 1 Schematic of the stepped cantilever piezoelectric energy harvester. (a) without cavity. (b), (c) and (d) are with rectangular cavity having different cavity thickness and position, (e) with trapezoidal cavity of taper angle $\alpha = 0.75^0$, (f) with trapezoidal cavity of taper angle $\alpha = 1.5^0$

3. Modelling of the energy harvesting structures

The model of energy harvesting structures shown in Fig. 1 is derived based on the Euler-Bernoulli beam theory with input applied at the free end of the beam using electromagnetic excitation. The model of the energy harvesting structure is developed by dividing the beam into three sections as shown in Fig. 2. In all the structures shown in Fig. 1, Section *I* and Section *III* consists of regular beam element. In the structure shown in Fig. 2(a), Section *II* consists of a rectangular cavity with a piezoelectric element bonded on its top and in Fig. 2(c) Section *II* consists of a trapezoidal cavity with a piezoelectric element bonded on its top.

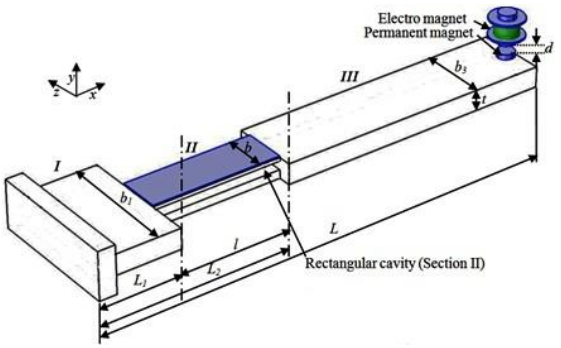

(a)

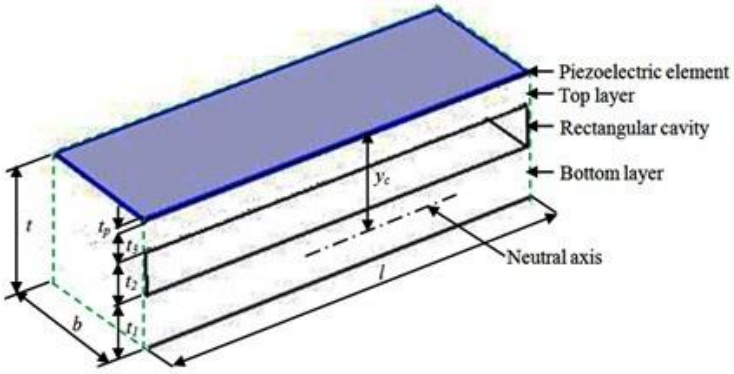

(b)

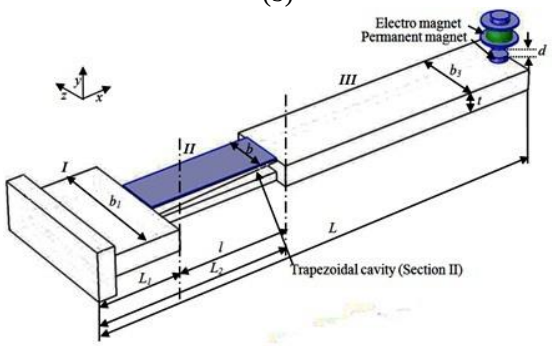

(c)

Continued-

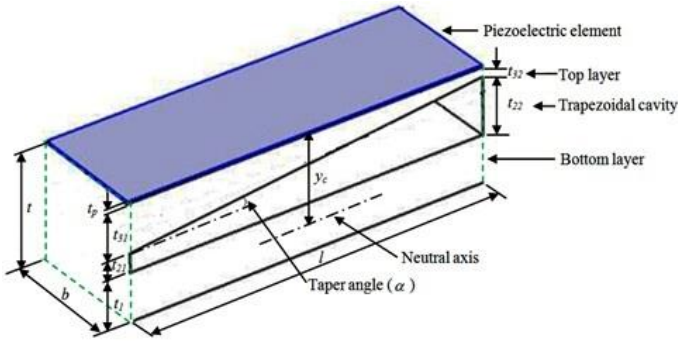

(d)

Fig. 2 (a) Schematic of the stepped cantilever piezoelectric energy harvester with rectangular cavity, (b) Section *II*, (c) Schematic of stepped cantilever piezoelectric energy harvester with trapezoidal cavity and (d) Section *II*.

The bending vibration equation for constant cross-section beam based on Euler–Bernoulli beam theory (Liao and Sodano 2012, Abdelkefi and Barsallo 2014) for the Section *I* and Section *III* is expressed as

$$\frac{d^4Y_1(x)}{dx^4} - \beta_1^4 Y_1(x) = 0, \quad (0 \le x \le L_1) \tag{1}$$

$$\frac{d^4Y_3(x)}{dx^4} - \beta_3^4 Y_3(x) = 0, (L_2 \le x \le L) \tag{2}$$

where $Y_1(x)$, $Y_3(x)$ are the amplitude of the modal functions of the Section *I*, Section *III*. $\beta_1^4 = \frac{\omega^2 m_1}{(EI)_1}$, ω is the fundamental angular frequency, m_1 is mass per unit length ($m_1 = \rho_b b_1 t$) and $(EI)_1$ is bending stiffness ($(EI)_1 = \frac{E_b b_1 t^3}{12}$) and b_1 is width of Section *I*. $\beta_3^4 = \frac{\omega^2 m_3}{(EI)_3}$, m_3 is mass per unit length ($m_3 = \rho_b b_3 t$), $(EI)_3$ is bending stiffness ($(EI)_3 = \frac{E_b b_3 t^3}{12}$) and b_3 is the width of Section *III*. where ρ_b, E_b and t are density, young's modulus and thickness of the beam.

The Section *II* of the beam with rectangular cavity shown in Figs. 1(b)-1(d) consists of four layers namely bottom layer (below the rectangular cavity), rectangular cavity, top layer (above the rectangular cavity) and piezoelectric element. The detailed schematic diagram of Section *II* with rectangular cavity is shown in Fig. 2(b).

The Section *II* of the stepped beam with trapezoidal cavity shown in Figs. 1(e)-1(f) consists of four layers namely, bottom layer (below the trapezoidal cavity), trapezoidal cavity, top layer (above the trapezoidal cavity) and piezoelectric element. The detailed schematic diagram of Section *II* is shown in Fig. 2(d). In Section *II* the length and width of all the layers are equal.

The vibration governing equation for the Section *II* is expressed as

$$\frac{d^4Y_2(x)}{dx^4} - \beta_2^4 Y_2(x) = 0, \quad (L_1 \le x \le L_2) \tag{3}$$

where $Y_2(x)$ is the amplitude of modal function and $\beta_2^4 = \frac{\omega^2 m_2}{(EI)_2}$ of Section *II*. For Section *II* having rectangular cavity, the mass per unit length is $m_2 = \sum_{i=1}^{n} \rho_i t_i b_i$, where ρ_i, t_i and b_i are density, thickness and width of the each layer respectively. The bending stiffness is, $(EI)_2 = \sum_{i=1}^{n} E_i I_i$, where E_i is the Young's modulus of each individual layer, I_i is the individual moment of inertia of each layer ($I_i = \frac{b_e t_i^3}{12} + b_e t_i (Z_G - Z_i)^2$), b_e is the equivalent width of the Section *II*. As all the layers in Section *II* having same width, the equivalent width b_e is equal to b (width of Section *II*) as shown in Fig. 2(b). Z_i is the location of neutral axis of each individual layer ($Z_i = \frac{t_i}{2} + \sum_{k=1}^{i-1} t_k$), Z_G is the location of the neutral axis of the Section *II* ($Z_G = \frac{\sum_{i=1}^{n} E_i A_i Z_i}{\sum_{i=1}^{n} E_i A_i}$), A_i is the cross-sectional area of the each individual layer ($A_i = b_e t_i$).

For the Section *II* of the beam having trapezoidal cavity mass per unit length, $m_2 = m(x)$, bending stiffness $(EI)_2 = EI(x)$. The thickness of the trapezoidal cavity is expressed as

$$t_2(x) = t_{21} + \alpha x, \qquad (0 \le x \le l) \tag{4}$$

where t_{21} is the trapezoidal cavity thickness towards the fixed end, α is taper angle($\alpha = \frac{t_{22} - t_{21}}{l}$), t_{22} is trapezoidal cavity thickness towards the free end of the beam. Thickness of the top layer is expressed as

$$t_3(x) = t - t_1 - t_2(x), \qquad (0 \le x \le l) \tag{5}$$

where, t_1 is the thickness of the bottom layer. For the Section *II* shown in Fig. 2(d), the location of neutral axis for each individual layer from the bottom surface of the beam and Moment of Inertia (MI) are found to be

$$\begin{aligned}
&\text{Neutral axis of bottom layer}, Z_1 = \frac{t_1}{2} \\
&\text{Neutral axis of trapezoid layer}, Z_2(x) = \frac{t_2(x)}{2} + t_1 \qquad (0 \le x \le l) \\
&\text{Neutral axis of top layer}, Z_3(x) = \frac{t_3(x)}{2} + t_2(x) + t_1 \qquad (0 \le x \le l) \\
&\text{Neutral axis of piezoelectric element}, Z_p = \frac{t_p}{2} + t
\end{aligned} \tag{6}$$

$$\begin{aligned}
&\text{MI of bottom layer}, I_1(x) = \frac{bt_1^3}{12} + bt_1[Z_G(x) - Z_1]^2 \\
&\text{MI of trapezoid layer}, I_2(x) = \frac{bt_2^3(x)}{12} + bt_2(x)[Z_G(x) - Z_2(x)]^2 \\
&\text{MI of top layer}, I_3(x) = \frac{bt_3^3(x)}{12} + bt_3(x)[Z_G(x) - Z_3(x)]^2 \\
&\text{MI of piezoelectric element}, I_p(x) = \frac{bt_p^3}{12} + bt_p[Z_G(x) - Z_p]^2
\end{aligned} \tag{7}$$

The location of the neutral axis of the Section *II*, $Z_G(x)$ is derived to be

$$Z_G(x) = \frac{E_b\{0.5t_1^2 + t_3(x)[0.5t_3(x) + t_2(x) + t_1]\} + E_p t_p(0.5t_p + t)}{E_b[t_1 + t_3(x)] + E_p t_p} \qquad (0 \le x \le l) \tag{8}$$

where b is the width of Section *II*, E_p and t_p are young's modulus and thickness of the piezoelectric element. The stiffness $EI(x)$ and mass per unit length $m(x)$ of Section *II* is given by

$$EI(x) = E_b[I_1(x) + I_3(x)] + E_p I_p(x) \tag{9}$$

$$m(x) = b\{\rho_b[t_1 + t_3(x)] + \rho_p t_p\} \tag{10}$$

The free vibration solutions for the Section *I*, Section *II* and Section *III* are expressed as

$$Y_1(x) = C_1 \sin\beta_1 x + C_2 \cos\beta_1 x + C_3 \sinh\beta_1 x + C_4 \cosh\beta_1 x, \quad (0 \le x \le L_1) \tag{11}$$

$$Y_2(x) = C_5 \sin\beta_2 x + C_6 \cos\beta_2 x + C_7 \sinh\beta_2 x + C_8 \cosh\beta_2 x, \quad (L_1 \le x \le L_2) \tag{12}$$

$$Y_3(x) = C_9 \sin\beta_3 x + C_{10} \cos\beta_3 x + C_{11} \sinh\beta_3 x + C_{12} \cosh\beta_3 x, \quad (L_2 \le x \le L) \tag{13}$$

where $C_1 - C_{12}$ are the constants of integration determined by suitable boundary and continuity conditions (Wang and Wu 2012, Salehi-Khojin *et al*. 2008). The forced vibration solution for the complete beam due to the dynamic force $f(x,t) = F\sin(\omega' t)\delta(x - L)$ applied at its free end is expressed as (Wang and Wu 2012, Park *et al.* 2012)

$$y_{1,2,3}(x,t) = Y_{1,2,3}(x)\frac{FY_3(L)\sin(\omega' t)}{\int_0^L Y_{1-3}(x)dx(\omega^2 - \omega'^2)} \tag{14}$$

where, $Y_{1,2,3}(x) = Y_1(x) + Y_2(x) + Y_3(x)$, $\int_0^L Y_{1-3}(x)dx = \int_0^{L_1} Y_1(x)dx + \int_{L_1}^{L_2} Y_2(x)dx + \int_{L_2}^{L} Y_3(x)dx$, $\delta(x - L)$ is the Dirac delta function to model point force and F, ω' are the magnitude and angular frequency of input force respectively. The voltage generated from the piezoelectric element at fundamental natural frequency is $V_g(t)$ (Wang and Wu 2012, Dosch *et al.* 1992)

$$V_g(t) = -\frac{e_{31} b y_c}{C_v} \frac{FY_3(L)}{\int_0^L Y_{1-3}(x)dx(\omega^2 - \omega'^2)} \left(\left.\frac{dY_2(x)}{dx}\right|_{x=L_2} - \left.\frac{dY_2(x)}{dx}\right|_{x=L_1} \right) \sin(\omega' t) \tag{15}$$

where e_{31} is the piezoelectric constant, C_v is the capacitance of the piezoelectric element. The perpendicular distance (y_c) from the beam neutral axis to the middle of the piezoelectric element is derived for Section *II* as, $y_c = t + \frac{t_p}{2} - Z_G$. Hence, y_c for the Section *II* having rectangular cavity is found to be

$$y_c = \frac{E_b(t_1^2 + t_3^2 + t_1 t_p + t_3 t_p + 2t_1 t_2 + 2t_1 t_3)}{2(E_b(t_1 + t_3) + E_p t_p)} \tag{16}$$

where t_1, t_2 and t_3 are the thickness of bottom layer, rectangular cavity and top layer of Section *II*. The perpendicular distance (y_c) from the beam neutral axis to the middle of the piezoelectric element for the Section *II* having trapezoidal cavity is found to be

$$y_c = t + 0.5t_p - \frac{E_b[3t_1 t_{21} + 3(t_1 + t_{21})(t_{31} + t_{32}) + t_{31}^2 + t_{32}^2 + t_{31} t_{32}] + 6E_p t_p (t + 0.5t_p)}{E_b[6t_1 + 3(t_{31} + t_{32})] + 6E_p t_p} \tag{17}$$

The magnitude of the dynamic force *F* at the free end of the beam (Challa *et al.* 2011), is given by

$$F = \frac{NIAB_r}{2L_e} \left(\frac{L_r + d}{\sqrt{R^2 + (L_r + d)^2}} - \frac{d}{\sqrt{R^2 + d^2}} \right) \tag{18}$$

where, *N* is number of coil turns, *I* is magnitude of current to the coil, *A* is the cross sectional area of core, B_r is the flux density of the permanent magnet, L_e is the length of the electromagnet, L_r is the length of the permanent magnet, *R* is the radius of the permanent magnet and *d* is the initial gap between the magnets as shown in Fig. 2(a) and 2(c). The optimum load resistance (R_L) of the energy harvester for excitation at the open-circuit fundamental natural frequency is given by (Erturk 2009)

$$R_L = \frac{1}{\omega C_v} \left[\frac{1 - \zeta^2 + (\gamma / 2\zeta)^2}{(1 + \gamma - \zeta^2)(1 + \gamma - 2\zeta^2)} \right]^{1/2} \tag{19}$$

where, ζ is damping ratio ($\zeta = \frac{(B^2 - 4AC)^{1/2} - B}{2A}$), A, B and C are coefficients. $A = 4(1 + \upsilon^2)$, $B = 4\gamma\upsilon$, $C = \upsilon^2\gamma^2 - \left(\frac{\gamma\upsilon\sigma}{|\hat{\alpha}(1)|\tilde{\theta}} \right)^2$. where the dimensionless terms are given by, $\upsilon = R_L C_v \omega$, $\gamma = \tilde{\theta}^2 / C_v \omega^2$, $\sigma = \frac{\sinh\lambda - \sin\lambda}{\cosh\lambda + \cos\lambda}$, $\lambda = 1.87510407$, $|\tilde{\alpha}(1)| = \frac{\gamma\upsilon|\sigma/\tilde{\theta}|}{\left[(2\upsilon\zeta)^2 + (2\zeta + \upsilon\gamma)^2\right]^{1/2}}$. Here,

$\tilde{\theta}$ is the electromechanical coupling is given by, $\tilde{\theta} = -e_{31} b y_c \left[\left. \frac{dY_2(x)}{dx} \right|_{x=L_2} - \left. \frac{dY_2(x)}{dx} \right|_{x=L_1} \right]$. The maximum value of power generated from the energy harvester (P_g) is given by (Dai *et al*. 2014a,b)

$$P_g = \frac{V_g^2}{R_L} \tag{20}$$

where, V_g is the maximum value of the generated voltage ($V_g(t)$) given by the Eq. (15).

4. Experimental evaluation

The energy harvesting structures shown in Fig. 1 are experimentally evaluated for its performance and compared with the results obtained from the model described in Section 3. The experimental setup for evaluating the proposed energy harvesting systems is shown in Fig. 3. The dimension and properties of the beams and piezoelectric element are given in Tables 1 and 2. The electromagnet has number of coil turns N = 2000, length L_e = 16 mm and cross sectional area A = 78 mm^2 is placed at the free end of the beam which is used to excite the beam. The flux density of the cylindrical permanent magnet B_r = 1.1 T, length L_r = 3 mm, radius R = 5 mm and the initial gap between the magnets d = 2.8 mm. The trapezoidal, rectangular cavities in the beams are made by wire cut EDM (Electric discharge machining) tool.

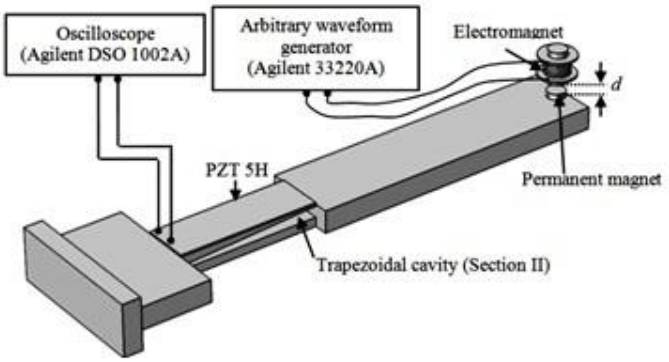

(a)

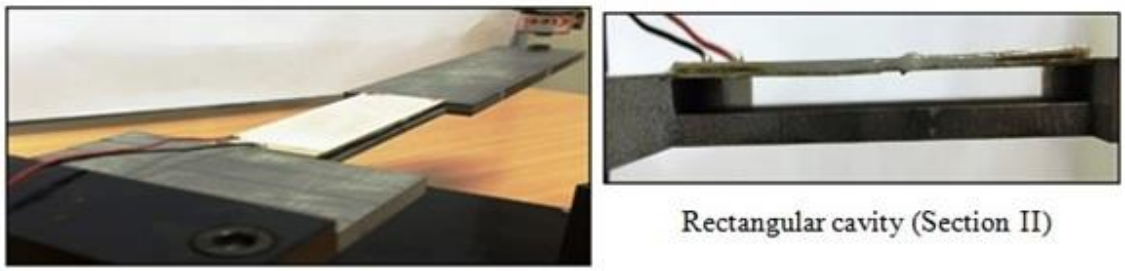

(b)

Continued-

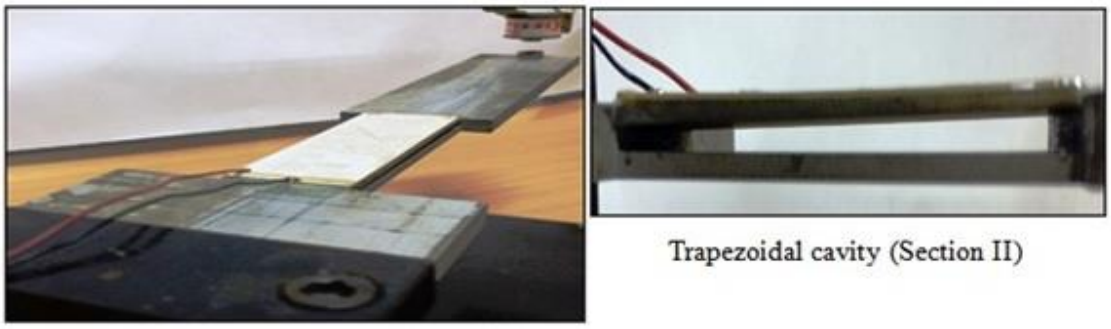

(c)

Fig. 3 Piezoelectric energy harvester with cavity beam. (a) Schematic of the experimental set up. (b) Photograph of the stepped beam with rectangular cavity and (c) Photograph of the stepped beam with trapezoidal cavity

Table 1 Dimension and properties of Aluminium beam

Symbol	Description	Value	Units
L	Length	276	mm
b_1	Width	72	mm
b	Width	25	mm
b_3	Width	40	mm
t_b	Thickness	6	mm
E_b	Young's modulus	71	GPa
ρ_b	Density	2700	Kg m^{-3}

Table 2 Dimension and properties of Piezoelectric element (PZT 5H)

Symbol	Description	Value	Units
l	Length	76	mm
b_p	Width	25	mm
t_p	Thickness	0.5	mm
E_p	Young's modulus	47.62	GPa
ρ_p	Density	7500	Kg m^{-3}
e_{31}	Piezoelectric constant	-16.6	C m^{-2}
d_{31}	Piezoelectric charge coefficient	-274	pC N^{-1}
C_v	Capacitance	104.3	nF

5. Results and discussions

In the energy harvesting structures shown in Fig. 1, the piezoelectric element is bonded on the top surface of the section *II* of the beam. The Section *II* is at a distance of 40 mm from the fixed end and width is 25 mm. The generated voltage for the stepped beam having a rectangular cavity with the thickness of 2 mm, positioned at a distance of 0.5 mm from the top surface of the beam as shown in Fig. 1(b) is computed. The shift in the neutral axis of the beam is found to be 0.612 mm and $y_c = 3.69$ mm. The shift in neutral axis of the beam for the cavity having a thickness of 3 mm positioned at 0.5 mm from the top surface of the beam shown in Fig. 1(c) is found to be 0.744 mm and $y_c = 3.83$ mm. The distance y_c, generated voltage and harvested power are found to increase with thickness of the cavity when placed at a fixed position from the top surface of the beam. The fundamental natural frequency is found to decrease with cavity thickness as shown in Fig. 4.

The voltage generated is computed by changing cavity position (1 mm) from the top surface of the beam for a thickness of 2 mm as shown in Fig. 1(d), the shift in the neutral axis of the beam is found to be 0.382 mm and $y_c = 3.46$ mm. The distance y_c, voltage generated and harvested power decreases when the position of the cavity moved away from the top surface of the beam with fixed cavity thickness. The fundamental natural frequency is found to increase with cavity position and the respective graphs are shown in Figs. 5(a)-5(c).

The generated voltage for the beam having a trapezoidal cavity with taper angle $\alpha = 0.75^0$ (t_{21}= 1 mm, t_{22}=2 mm), positioned at a distance of 2.5 mm from the bottom surface of the beam shown in Fig. 1(e) is computed from the model presented in Section 3. The shift in neutral axis of the beam is found to be 0.23 mm and y_c=3.33 mm. The shift in neutral axis of the beam having trapezoidal cavity with taper angle $\alpha = 1.5^0$ (t_{21}= 1 mm, t_{22}=3 mm), positioned at a distance of 2.5 mm from the bottom surface of the beam, shown in Fig. 1(f), is found to be 0.46 mm and y_c= 3.54 mm. The distance y_c, generated voltage and harvested power are found to be increasing with increase in angle of taper α of the trapezoidal cavity in the beam. The fundamental natural frequency of the harvester is found to be decreasing with increase in angle of taper α, the results are shown in Fig. 6.

The voltage-force characteristics for the stepped beam without cavity (shown in Fig. 1(a)), with rectangular cavity (shown in Figs. 1(b)-1(d)) are shown in Figs. 7 and 8. The results are also compared with the normal beam of equal width without cavity. For the vibration force of 0.1 to 0.4 N applied at the free end of the beam, the generated voltage is computed from Eq. (15) and measured from experimentation is found to be in close agreement in all cases. The increase in voltage is 1.61 and 2.95 times higher for the stepped beam having a cavity thickness of 2 mm and 3 mm positioned at a distance of 0.5 mm from the top surface of the beam as compared to the stepped beam without cavity. Moreover, as compared to the normal beam without cavity the increase in voltage is 1.7 and 3.1 times higher for the stepped beam having a cavity thickness of 2 mm and 3 mm positioned at a distance of 0.5 mm from the top surface of the beam.

The generated voltage from the stepped beam without cavity (shown in Fig. 1(a)), with trapezoidal cavity (shown in Figs. 1(e)-1(f)) for the input vibration force of 0.1 to 0.4 N applied at the free end of the beam computed from the model presented in Section 3 and measured from experimentation is shown in Fig. 9. Also the results are compared with the voltage generated from the normal beam of equal width. The generated voltage from the stepped beam with trapezoidal cavity having taper angle of $\alpha = 0.75^0$ and $\alpha = 1.5^0$ is 1.38 and 2.5 times higher as compared to the voltage generated from the stepped beam without cavity. Furthermore, as compared to the

normal beam without cavity the generated voltage is 2.03 and 3.7 times higher for the stepped beam with trapezoidal cavity having taper angle of $\alpha = 0.75^0$ and $\alpha = 1.5^0$.

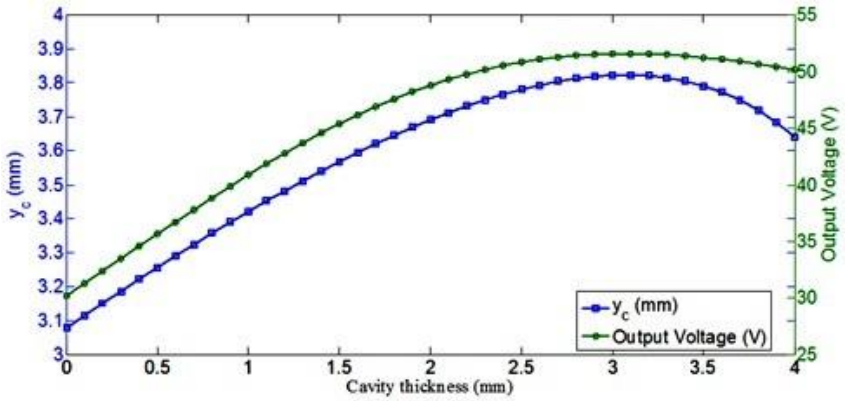

(a)

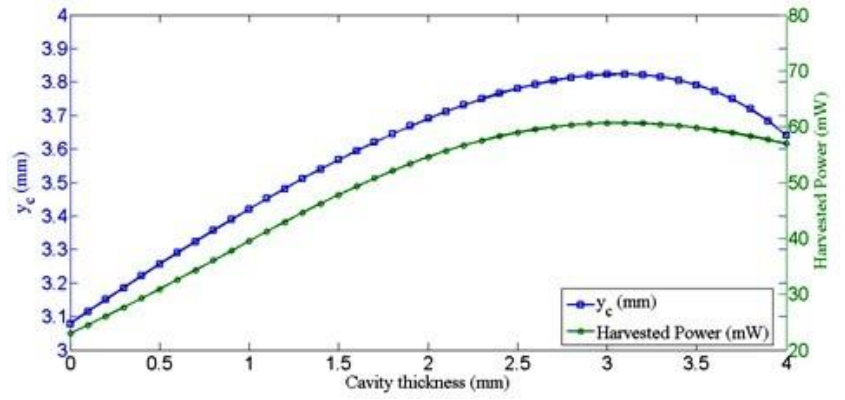

(b)

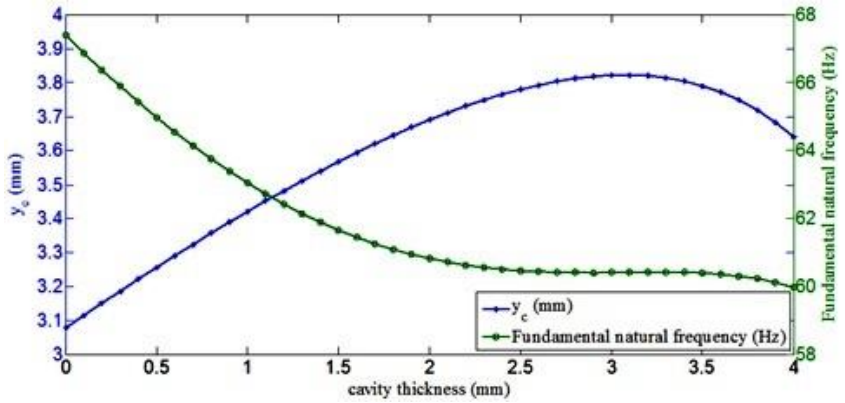

(c)

Fig. 4 Analytical results for variation in thickness of the cavity positioned at 0.5 mm, (a) Output Voltage, (b) Harvested Power and (c) Fundamental natural frequency

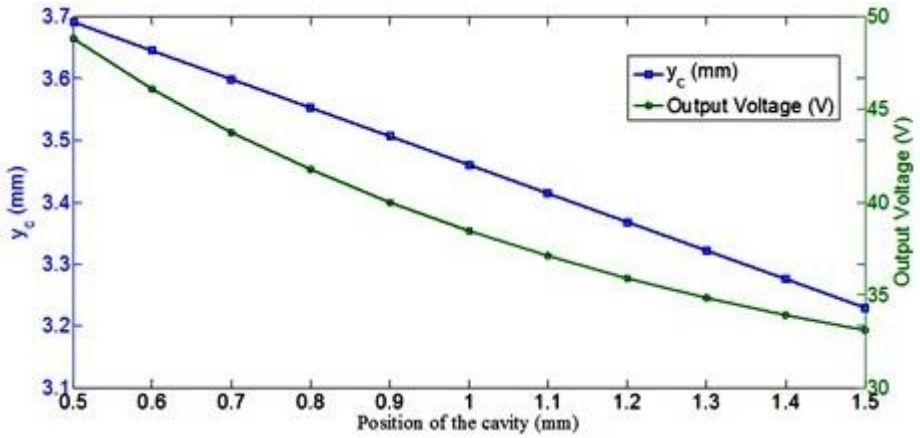

(a)

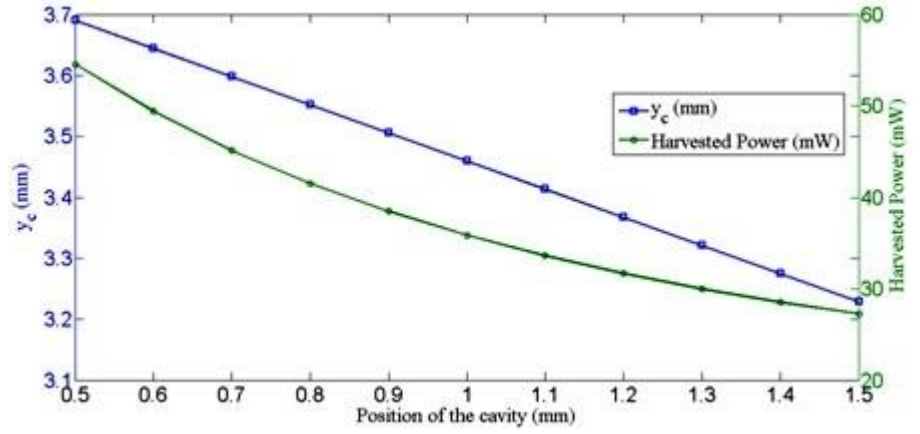

(b)

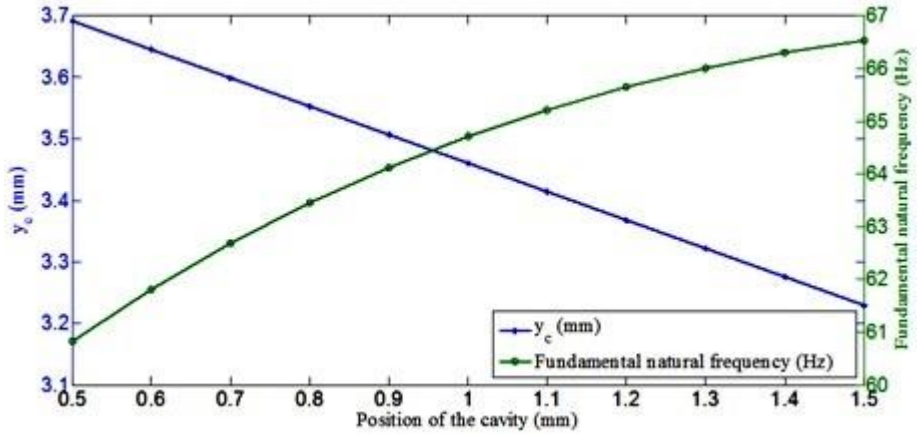

(c)

Fig. 5 Analytical results for variation in position of the cavity of 2 mm thickness. (a) Output Voltage. (b) Harvested Power and (c) Fundamental natural frequency

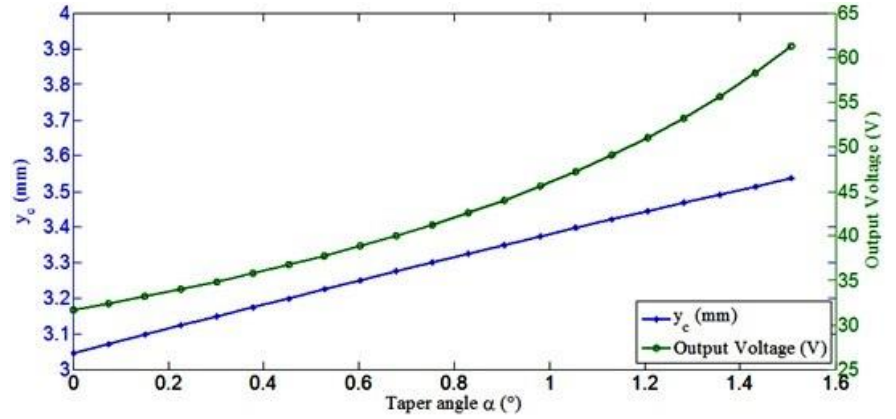

(a)

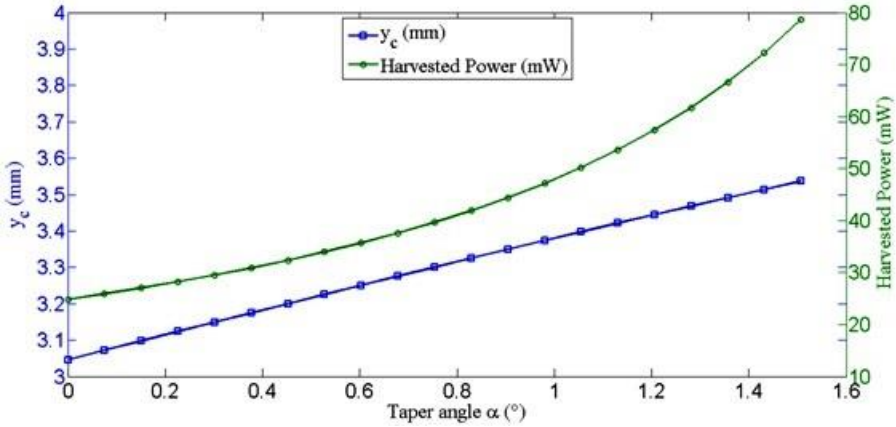

(b)

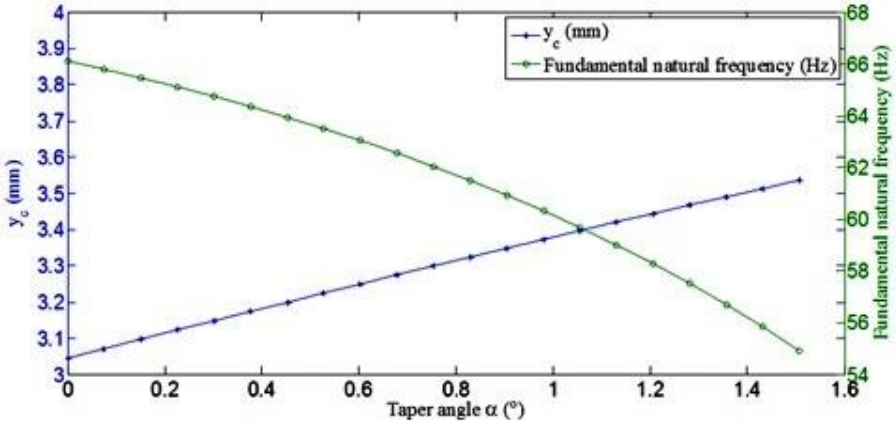

(c)

Fig. 6 Analytical results for variation in taper angle (α) of the trapezoidal cavity positioned at a distance of 2.5 mm from the bottom surface. (a) Output Voltage, (b) Harvested Power and (c) Fundamental natural frequency

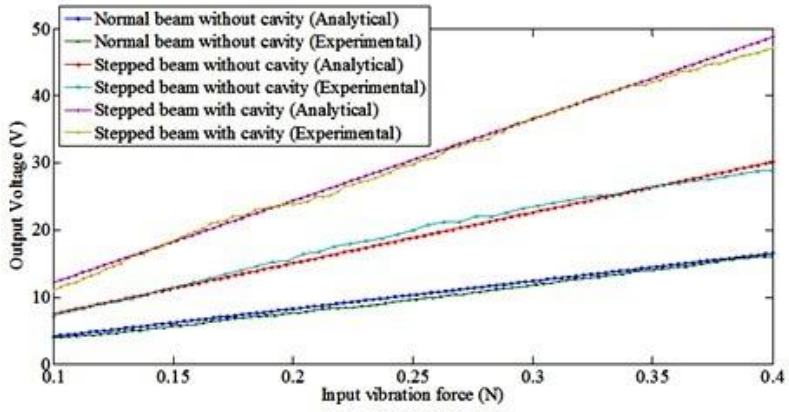

(a)

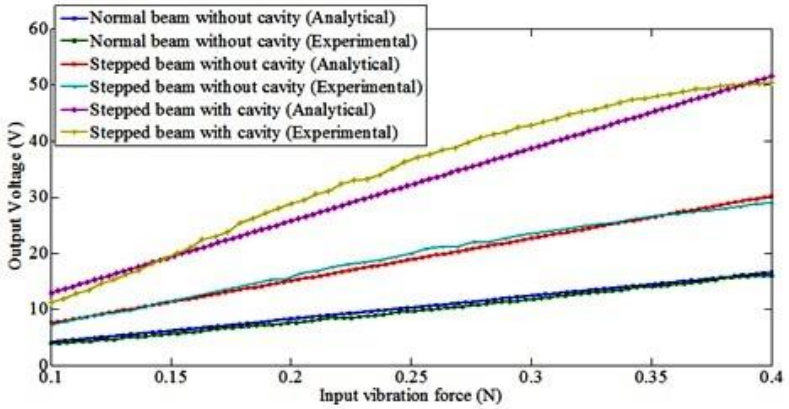

(b)

Fig. 7 Voltage- Force characteristics for the cavity positioned at 0.5 mm (a) For the cavity thickness of 2 mm and (b) For the cavity thickness of 3 mm

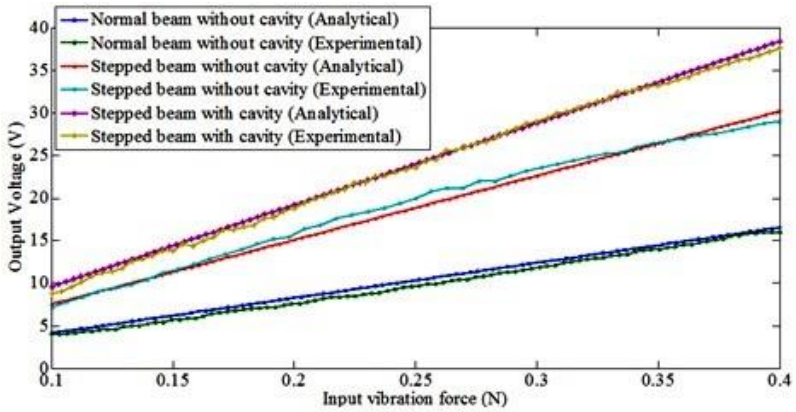

Fig. 8 Voltage- Force characteristics for 2 mm thick cavity positioned at 1mm

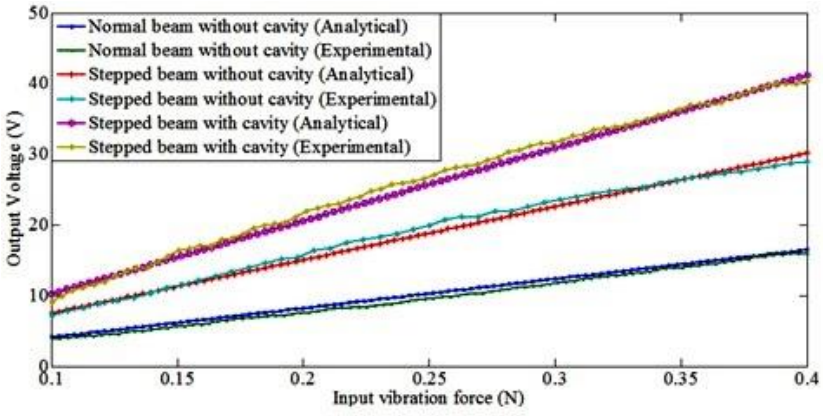

(a)

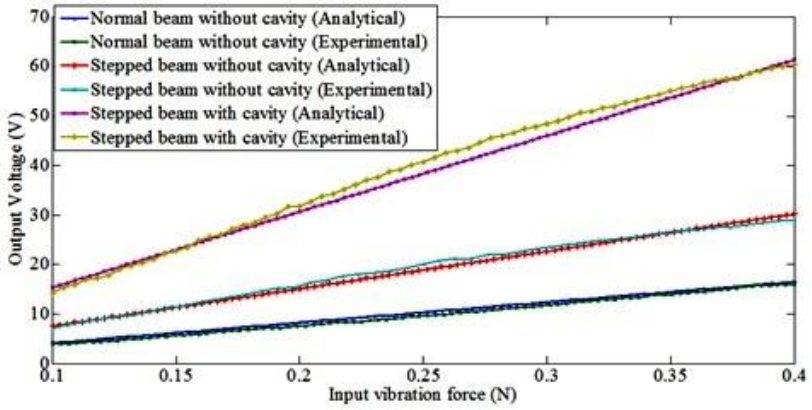

(b)

Fig. 9 Voltage-Force characteristics for the stepped with trapezoidal cavity positioned at a distance of 2.5 mm from the bottom surface. (a) Taper angle $\alpha = 0.75^0$ and (b) Taper angle $\alpha = 1.5^0$

6. Conclusions

This work aims at improving the energy harvested from the piezoelectric energy harvesting system by structural modification, with inclusion of rectangular and trapezoidal cavities. A stepped beam with rectangular cavity and trapezoidal cavity is proposed and it is demonstrated that, the generated voltage is higher in both the cases compared to stepped beam without cavity and normal beam without cavity. Analytical and experimental evaluations shows that the thickness, position of the rectangular cavity and the taper angle of the trapezoidal cavity has influenced on the neutral axis shift and hence the generated output voltage and power. From the analytical and experimentation results it can be concluded that simple modification(s) in the structure of the cantilever beam can improve the output voltage and harvested power of the piezoelectric energy harvester.

References

Abdelkefi, A. and Barsallo, N. (2014), "Comparative modelling of low-frequency piezomagnetoelastic energy harvesters", *J. Intel.Mat. Syst. Str.*, DOI:10.1177/1045389X14523860.

Abdelkefi, A. and Ghommem, M. (2013), "Piezoelectric energy harvesting from morphing wing motions for micro air vehicles", *Theor. Appl. Mech. Lett.*, **3**, 052001.

Abdelkefi, A., Nayfeh, A.H., Hajj, M.R. and Najar, F. (2012), "Energy harvesting from a multi frequency response of a tuned bending-torsion system", *Smart Mater. Struct.*, **21**(7), 075029.

Barker, S., Brennan, D., Wright, N.G. and Horsfall, A.B. (2011), "Piezoelectric-powered wireless sensor system with regenerative transmit mode", *Inst. Eng. Technol.*, **1**, 31-38.

Ben Ayed, S., Abdelkefi, A., Najar, F. and Hajj, M.R. (2014), "Design and performance of variable-shaped piezoelectric energy harvesters", *J. Intel. Mat. Syst. Str.*, **25**,174-186.

Benasciutti, D., Moro, L., Zelenika, S. and Brusa, E. (2010), "Vibration energy scavenging via piezoelectric bimorphs of optimized shapes", *Microsyst. Technol.*, **16**,657-668.

Carlos De Marqui, J, Erturk, A. and Inman, D.J. (2009), "An electromechanical finite element model for piezoelectric energy harvester plates", *J. Sound Vib.*, **327**, 9-25.

Challa, V.R., Prasad, M.G. and Fisher, F.T. (2011), "Towards an autonomous self-tuning vibration energy harvesting device for wireless sensor network applications", *Smart Mater. Struct.*, **20**(2), 025004.

Chen, X.R., Yang, T.Q., Wang, W. and Yao, X. (2012), "Vibration energy harvesting with a clamped piezoelectric circular diaphragm", *Ceram. Int.*, **38**, 271-S274.

Dai, H.L., Abdelkefi, A. and Wang, L. (2014a), "Piezoelectric energy harvesting from concurrent vortex-induced vibrations and base excitations", *Nonlinear Dynam*, **77**(3), 967-981.

Dai, H.L., Abdelkefi, A. and Wang, L. (2014b), "Theoretical modeling and nonlinear analysis of piezoelectric energy harvesting from vortex-induced vibrations", *J. Intel. Mat. Syst. Str.*, 1-14.

Dosch, J.J., Inman, D.J. and Garcia, E. (1992), "A self-sensing piezoelectric actuator for collocated control", *J. Intel. Mat. Syst. Str.*, **3**, 166-185.

Ece, M.C., Aydogdu, M. and Taskin, V. (2007), "Vibration of a variable cross-section beam", *Mech. Res. Commun.*, **34**(1), 78-84.

Erturk, A. (2009), *Electromechanical modeling of piezoelectric energy harvesters*, PhD Dissertation, Virginia Tech, Blacksburg.

Ferrari, M., Ferrari, V., Guizzetti, M. and Marioli, D. (2009), "An autonomous battery- less sensor module powered by piezoelectric energy harvesting with RF transmission of multiple measurement signals", *Smart Mater. Struct.*, **18**, 085023.

Guan, Q.C., Ju, B., Xu, J.W., Liu, Y.B. and Feng, Z.H. (2013), "Improved strain distribution of cantilever piezoelectric energy harvesting devices using H-shaped proof masses", *J. Intel. Mat. Syst. Str.*, **24**(9), 1059-1066.

Kim, N.L., Jeong, S.S., Cheon, S.K. and Park, T.G. (2013), "Generating characteristics of hollow-plate-type piezoelectric energy harvester", *J. Korean Phys. Soc.*, **63**, 2310-2313.

Levron, Y., Shmilovitz, D. and Martinez-Salamero, L. (2011), "A power management strategy for minimization of energy storage reservoirs in wireless systems with energy harvesting", *IEEE T. Circuits Syst.*, **58**(3), 633-643.

Li, W.G., He, S. and Yu, S. (2010), "Improving power density of a cantilever piezoelectric power harvester through a curved L-shaped proof mass", *IEEE T. Ind. Electron.*, **57**(3), 868-876.

Liao, Y. and Sodano, H.A. (2012), "Optimal placement of piezoelectric material on a cantilever beam for maximum piezoelectric damping and power harvesting efficiency", *Smart Mater. Struct.*, **21**(10), 105014.

Magoteaux, K.C., Sanders, B. and Sodano, A.H. (2008), "Investigation of energy harvesting small unmanned air vehicle", *Smart Materials and Structures: Active and Passive Smart Structures and Integrated Systems II, Proceedings of the SPIE, San Diego, CA.*

Mehraeen, S., Jagannathan, S. and Corzine, K.A. (2010), "Energy harvesting from vibration with alternate scavenging circuitry and tapered cantilever beam", *IEEE T. Ind. Electron.*, **57**(3), 820-830.

Paquin, S. and St-Amant, Y. (2010), "Improving the performance of a piezoelectric energy harvester using a variable thickness beam", *Smart Mater. Struct.*, **19**(10), 105020 (14pp).
Park, J., Lee, S. and Kwak, B.M. (2012), "Design optimization of piezoelectric energy harvester subject to tip excitation", *J. Mech. Sci. Technol.*, **26**(1), 137-143.
Priya, S. (2007), "Advances in energy harvesting using low profile piezoelectric transducers", *J. Electroceram*, **19**, 165-182.
Salehi-Khojin, A., Bashash, S. and Jalili, N. (2008), "Modeling and experimental vibration analysis of nano mechanical cantilever active probes", *J. Micromech. Microeng.*, **18**(8), 085008.
Sodano, H.A. and Inamn, D.J. (2004), "A review of power harvesting from vibration using piezoelectric materials", *Shock Vib. Digest*, **36** (3), 197-205.
Wang, Q. and Wu, N. (2012), "Optimal design of a piezoelectric coupled beam for power harvesting", *Smart Mater. Struct.*, **21**(8), 085013.

BS